

Microstructural Evolution in Triaxial Porcelain

Yaseen Iqbal and William Edward Lee*

Department of Engineering Materials, University of Sheffield, Sheffield S1 3JD, United Kingdom

Microstructural evolution in a model triaxial porcelain was studied by X-ray diffractometry and electron microscopy of quenched samples after firing for 3 h at 600°–1500°C. The clay component dehydroxylated to metakaolin at ~550°C. Metastable sanidine formed from decomposition of the feldspar at >600°C and dissolved at >900°C. Liquid formation at ~1000°C was associated with melting of feldspar and silica discarded from metakaolin formation via the K₂O–Al₂O₃–SiO₂ eutectic. Liquid content increased at 1000°–1200°C with further feldspar melting and additionally at >1200°C because of quartz dissolution. Small (≤7 nm) mullite and γ-alumina crystals precipitated in pure clay relicts and larger (≤30 nm) mullite crystals in mixed clay-feldspar relicts at 1000°C. In the evolving microstructures, three regions were observed. These regions were derived from pure clay relicts containing primary (type-I) mullite; feldspar-penetrated clay relicts, also containing secondary (granular type-II) mullite; and the matrix of fine clay, feldspar, and quartz, containing secondary (granular type-II and elongated type-III) mullite. In addition to shape, the mullite size changed, increasing from regions containing type-I to type-III mullite, because the increasingly fluid liquid enhanced crystal growth. Below 1300°C, primary mullite was richer in Al₂O₃ than the secondary mullite, and the glass composition was inhomogeneous, with the K₂O and Al₂O₃ contents varying throughout the microstructure. Above 1400°C, mullite began to dissolve.

I. Introduction

TRIAxIAL porcelain bodies have been studied extensively.^{1–4} These porcelain bodies are typically fired mixtures of 50 wt% fine-grained clay (commonly kaolin, Al₂(Si₂O₅)(OH)₄), 25 wt% flux (usually feldspar), and 25 wt% filler (commonly quartz). The evolution of the microstructure of porcelains to their final state is known in general terms.^{5,6} The clay provides plasticity, allowing easy shape formation, and acts as a binder for the other body components when they are in the green state. At the beginning of sintering, kaolin clay shrinks and cracks. At 500°–600°C, the clay dehydroxylates to form metakaolin, within which γ-Al₂O₃ spinel nucleates at >900°C.⁷ At ~1000°C, decomposition of clay relicts forms fine (<0.5 μm) primary mullite.⁸ Lundin⁵ and Schuller⁹ reported the formation of two types of mullite crystals in porcelain bodies, distinguished by their size. Aggregates of small (<0.5 μm) mullite crystals coming from the clay relicts are referred to as *primary* mullite, whereas the long (>1 μm) needle-shaped mullite crystals observed in the feldspar melt are termed *secondary* mullite. Iqbal and Lee⁶ used electron microscopy and energy-dispersive X-ray spectroscopy of commercial porcelains to show that the Al₂O₃:SiO₂ ratio of cuboidal primary mullite (<0.5 μm) was close to 2:1 (i.e., Al₂O₃-rich), while it was ~3:2 for elongated

(>1 μm) secondary mullite and was related to the varying Al₂O₃ content in clay and feldspar relicts. Furthermore, the increase in mullite crystal size from the clay-feldspar relict interface to the feldspar relict center was related to matrix viscosity, arising from varying K₂O content. Schuller⁹ used electron microscopy to show that all primary mullite transforms to secondary mullite at 1400°C and, because of the complete dissolution of quartz, a texture consisting of glass and mullite needles results. It was also shown that cristobalite crystallizes in some, but not all clays, at ~1225°C.¹⁰

Feldspars are low-melting mineral alkali aluminosilicates and serve to lower the temperature at which viscous liquid forms. The liquid phase reacts with other body constituents and gradually permeates the microstructure, leading to its densification. Feldspars of major commercial interest are potash feldspar (K₂O·Al₂O₃·0.6SiO₂), soda feldspar (Na₂O·Al₂O₃·0.6SiO₂), and lime feldspar (CaO·Al₂O₃·0.2SiO₂).¹¹ Potash feldspar crystallizes in the monoclinic form as orthoclase and in the triclinic form as microcline, while soda and lime feldspars crystallize as triclinic albite and anorthite, respectively.⁸ The body vitrification temperature decreases with increase in feldspar content.¹² Nepheline syenite is predominantly microcline (KAISi₃O₈), along with ~10 vol% nepheline (Na₃KAl₄Si₄O₁₆), and is commonly used as a flux in modern pottery bodies. Feldspar is believed to melt at ~1100°C in the contact zone between feldspar crystals and clay relicts, and the amorphous silica discarded from clay relicts during metakaolin formation may assist melt formation at ~985°C via the 9.5K₂O·10.9Al₂O₃·79.8SiO₂ (in wt%) eutectic.¹³ Potash feldspar never crystallizes from its own melt and is known to dissociate into glass and leucite (KAISi₂O₆) at ~1170°C. Leucite crystals (alone) are known to dissolve at 1530°C.¹⁰ Sanidine ((Na,K)AlSi₃O₈) formation has been reported in mixed alkali feldspars heated at 900°–1050°C, but not in porcelain compositions.¹⁴ Clay and feldspar also contain small amounts of oxides, such as Na₂O, CaO, MgO, TiO₂, and Fe₂O₃, which may influence the crystallization behavior and vitrification temperature of the body and the glass viscosity.¹⁰

Fillers (such as quartz) are materials of high melting temperature that are chemically resistant at commercial firing temperatures (<1300°C). They reduce the tendency of the body to warp, distort, or shrink when it is fired to temperatures resulting in substantial quantities of viscous glass.¹⁵ The low-temperature form of quartz (α) inverts to high-temperature form (β) at 573°C. Below 1250°C, quartz is considered relatively insoluble;¹⁶ above 1250°C, dissolution of quartz forms silica-rich amorphous solution rims around quartz grains. Dissolution of quartz depends on its size: i.e., coarser quartz dissolution is slower than that of fine grains.² Quartz grains <20 μm completely dissolve at ~1350°C, and at >1400°C, porcelain bodies consist almost entirely of mullite and glass, with little quartz. Cracks commonly observed in and around large quartz grains occur because of the large thermal expansion mismatch between the crystalline quartz (α ≈ 23 × 10⁻⁶ K⁻¹) and the glassy phase (α ≈ 3 × 10⁻⁶ K⁻¹) in the temperature range 20°–750°C.^{15,17} Ohya *et al.*¹⁸ used acoustic emission to demonstrate that quartz cracked in the temperature range 900°–800°C on cooling from 1200°C, because of its negative thermal expansion at >1000°C and a lack of stress relaxation in the glass. Lundin^{5,15} reported that if enough quartz is present to saturate the melt with

M. Grutzeck—contributing editor

Table I. Chemical Compositions of Raw Materials Used[†]

Raw material	SiO ₂	Al ₂ O ₃	Fe ₂ O ₃	CaO	Na ₂ O	K ₂ O	MgO	TiO ₂
Nepheline syenite	55.8	23.7	0.105	1.6	7.9	8.9		
Kaolin (ECC Intl.)	48	37	0.77	0.07	0.1	2.3	0.3	0.03
Silica sand	99.8	0.05	0.009	0.02	0.05	0.01	0.05	

[†]All compositions in wt%; data from supplier.

Table II. Relevant Crystallographic Data

Phase	Crystal system	Space group	Lattice parameters (Å and °)						ICDD File No.
			<i>a</i>	<i>b</i>	<i>c</i>	α	β	γ	
α -quartz	Hexagonal	<i>P</i> ₃ ₂ ₁	4.91	4.91	5.40	90	90	120	5-490
Microcline	Triclinic	<i>C</i> 1	8.57	12.96	7.2	89.4	115.5	90.5	22-675
Nepheline	Hexagonal	<i>P</i> 6 ₃	10.01	10.01	8.40	90	90	120	9-458
Leucite	Tetragonal	<i>I</i> 4 ₁ / <i>a</i>	13.06	13.06	13.751	90	90	90	15-47
Kaolinite	Triclinic	<i>P</i> 1	5.155	8.95	7.40	91.68	104.87	89.9	14-164
Sanidine	Monoclinic	<i>C</i> 2/ <i>m</i>	8.42	13.0	7.16	90	116.1	90	19-1227
Mullite	Orthorhombic	<i>P</i> <i>b</i> <i>a</i> <i>m</i>	7.545	7.689	2.884	90	90	90	15-776
Cristobalite	Tetragonal	<i>P</i> 4 ₁ 2 ₁ 2	4.971	4.971	6.918	90	90	90	11-695

silica, its dissolution stops and it transforms partially into cristobalite. Initiation of cristobalite formation at the quartz-melt interface and its growth into the quartz grains suggests that it depends on the presence of the melt.

The final microstructures of fired porcelain bodies consist of 10%–25% mullite, with composition ranging from 2Al₂O₃·1SiO₂ to 3Al₂O₃·2SiO₂, 5%–25% α -quartz (SiO₂), and 0%–8% pores dispersed in 65%–80% potassium aluminosilicate glass. Bodies with a high percentage of quartz also may contain cristobalite.^{5,15} Processes such as densification behavior, homogeneity of the body, and shrinkage mechanisms during firing can be observed by studying the microstructures and are of greater commercial interest to the whitewares industry. The purpose of the present study was to investigate microstructural changes in model porcelain bodies as they evolve on firing, by quenching samples at temperatures from 600° to 1500°C using X-ray diffractometry (XRD), scanning electron microscopy (SEM), transmission electron microscopy (TEM), and energy-dispersive spectroscopy (EDS).

II. Experimental Procedure

Model porcelain bodies were prepared by mixing 55 wt% quality china clay (kaolin) (ECC International, Cornwall, U. K.) and 15 wt% North Cape nepheline syenite (Bayer, Ltd., Newbury, U. K.) with 30 wt% silica (Tilcon (South), Ltd., Stoke-on-Trent, U. K.). The chemical compositions of the raw materials used are given in Table I. The quoted sizes of the clay, feldspar, and quartz particles were 0.2–6 μ m, 10–50 μ m, and 180–250 μ m, respectively. Batches (300 g each) were wet-milled in a porcelain mill with zirconia media for 6 h at 80 rpm. To disperse clay agglomerates, the slurry was further milled for 30 min after the addition of 3 g of deflocculant (Dispex N40, Allied Colloids, Ltd., Bradford, U. K.). The slurry was passed through a 212 μ m mesh, oven-dried overnight at 100°C, powdered in a porcelain mortar and pestle, and again sieved through a 212 μ m mesh. The resulting powders were moistened by spraying with a fine mist of distilled water droplets (10 wt%) and granulated by hand over a polyethylene sheet. The granulates were pressed at ~40 MPa in a steel die and the pellets (0.9 cm \times 2.5 cm) fired in mullite or alumina crucibles at 100°C intervals from 600° to 1500°C at 10°C/min, soaked for 3 h at temperature, and cooled to room temperature at ~75°C/min. These samples are referred to as P0, P600, and P1500 throughout this study, where P0 is the as-mixed body and the number after P denotes the relevant firing temperature.

The apparent density of the as-pressed pellets was calculated from measurements made using Vernier calipers and a digital balance. Bulk densities of the fired pellets were determined using

a mercury densitometer (Model No. P1210, Mettler-Toledo, Inc., Hightstown, NY).

Differential thermal analysis (DTA) was performed on the as-mixed porcelain and the nepheline syenite powder, using a Stanton Redcroft Standata (Model No. 673-4, The Fine Work Co., Ltd., Sutton, U.K.) DTA unit. Calcined alumina was used as a reference. For XRD, powdered porcelain bodies and fired and unfired nepheline syenite powder were scanned with CuK α radiation from 10° \leq 2θ \leq 60° at a scanning speed of 0.5°/min, using a diffractometer (Model No. PW1730/10, Philips Electronic Instruments, Mahwah, NJ) operating at 30 mA and 50 kV. The diffractometer was calibrated with an α -quartz standard. The ICDD files[†] listed in Table II were used to identify crystalline phases.

SEM samples were polished to a 0.25 μ m finish with diamond pastes after initial grinding with SiC powder and water. The polished surfaces of samples fired to \geq 1000°C were etched by dipping for 3 min in a 5% HF solution, washing in water and acetone, and subsequently carbon coating (Model No. Speedivac 12E6/1598, Edwards High Vacuum Products, Crawley, W. Sussex, U. K.). An SEM (Model No. JEOL 6400, JEOL, Tokyo, Japan) operating at 20 kV was used for microstructural examination of the samples. Secondary electron images (SEI), back-scattered electron images (BSI), and EDS (Model No. 6276, Link Analytical Systems, High Wycombe, Buckinghamshire, U. K.) were used to identify the constituent phases.

Standard TEM sample preparation procedures were followed that involved grinding, polishing, dimpling, argon-ion-beam thinning, and carbon coating. Samples fired to temperatures <1000°C could not be thinned using standard techniques, so that powders of these samples were suspended in acetone and deagglomerated by ultrasonic treatment. A carbon film supported on a copper grid was dipped in the slurry and dried in air, leaving particles suspended on the carbon film. A TEM (Model No. 420, Philips) operating at 120 kV and a TEM (Model No. JEOL 3010, JEOL) operating at 300 kV were used for bright-field (BF) imaging and selected area diffraction (SAD). A single-crystal silicon sample was used as the standard for camera constant (λL) calibration, where λ is the electron wavelength and L the camera length. At least three SAD patterns (SADPs) from each crystal identified were indexed. The elemental compositions of crystals and matrix glass were analyzed using EDS (Model No. 6618, Link Analytical) with a JEOL 3010 TEM. Precise quantification of the EDS spectra from the mullite crystals was difficult because of their overlap with glass, although

[†]International Centre for Diffraction Data, Newtown Square, PA.

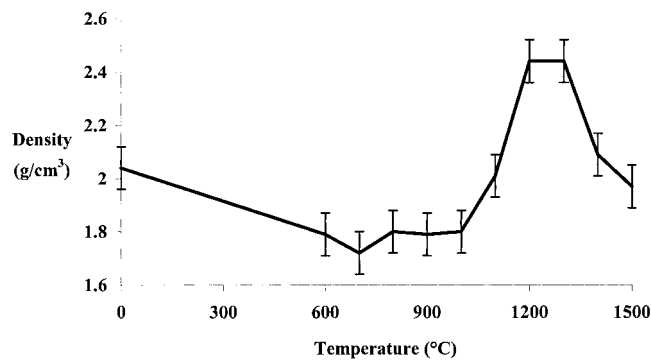


Fig. 1. Variation in density of porcelain bodies after 3 h at temperature.

attempts were made to obtain spectra from crystals with little overlapping glass from ~50 regions of each phase.

III. Results

The density of the samples reached a maximum (2.44 g/cm³) after quenching from 1200° or 1300°C, above which temperature the density decreased continuously, reaching a minimum (1.97 g/cm³) at 1500°C (Fig. 1). DTA from the as-mixed porcelain powder (P0) was similar to that from kaolinite, with an endotherm at ~550°C, indicating clay dehydroxylation, and an exotherm at ~1000°C, resulting from mullite crystallization. As expected, DTA of nepheline syenite revealed no peaks, but just a continuous endothermic drift at >500°C, because of its gradual sintering and/or melting. XRD of unfired nepheline syenite powders revealed microcline, along with a small proportion (<10 vol%) of nepheline. After the nepheline syenite was quenched from 1200°C, three small leucite peaks were detected at $2\theta = 25.9^\circ$, 27.32° , and 31.66° , although a large amorphous hump indicated that the composition was ~95% glass. The leucite peaks disappeared by 1400°C, indicating dissolution of leucite in the glass.

The phases detected by XRD in the as-mixed and fired porcelain bodies are listed in Table III. The as-mixed samples contained kaolinite, α -quartz, and microcline, along with a small proportion (~5 vol%) of nepheline. XRD peaks resulting from kaolinite disappeared at some temperature <600°C because of the loss of OH⁻ groups from the structure, leaving α -quartz, microcline, and nepheline in P600. Microcline and nepheline were present up to 1100°C, but disappeared at higher temperatures, presumably when they dissolved. The appearance of the (202) sanidine peak (at $2\theta \approx 27.18^\circ$) at ~700°C suggested that the sanidine formed between 600° and 700°C, increasing in amount to 900°C, above which it disappeared. Several other small peaks on the XRD traces from samples fired at 700°–900°C matched sanidine, but overlap with other feldspar peaks made unambiguous identification difficult. The decreased intensity of the α -quartz peaks at >1200°C showed the partial dissolution of α -quartz at

Table III. Constituents of Porcelain Body Held 3 h at Various Temperatures

Temperature (°C)	Constituent phases
Unfired	α -quartz, kaolinite, microcline, nepheline
600	α -quartz, microcline, nepheline
700	α -quartz, microcline, nepheline, sanidine
800	α -quartz, microcline, nepheline, sanidine
900	α -quartz, microcline, nepheline, sanidine
1000	α -quartz, microcline, nepheline
1100	α -quartz, microcline, nepheline, mullite, glass
1200	α -quartz, mullite, glass
1300	α -quartz, mullite, glass
1400	α -quartz, mullite, glass
1500	α -quartz, mullite, cristobalite, glass

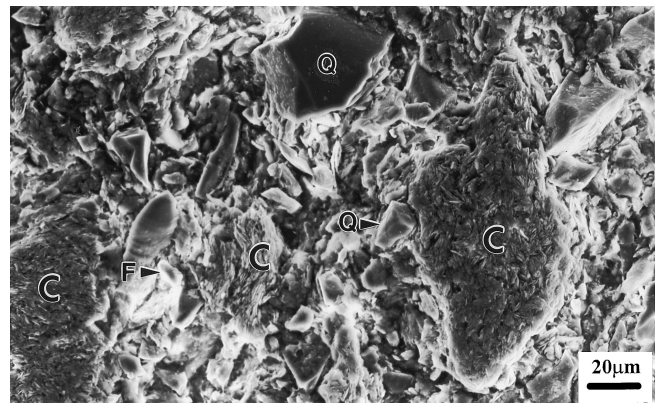


Fig. 2. SEI of unetched P700, showing α -quartz grains ("Q"), clay relict agglomerates ("C"), and feldspar grains ("F").

higher temperatures. Mullite was detected at 1100°C; its amount increased to a maximum at 1400°C, before decreasing at higher temperatures. This behavior indicated that mullite formed at >1000°C and partially dissolved at >1400°C. A single cristobalite peak (at $2\theta \approx 21.96^\circ$) suggested it formed at 1500°C.

TEM analysis of the as-mixed porcelain powder (P0) revealed pseudo-hexagonally shaped kaolinite crystals, elongated microcline crystals, and irregular nepheline crystals. Figure 2 is an SEI of P700, showing agglomerates of dehydroxylated clay (labeled "C") ($\leq 90 \mu\text{m}$) and irregular ($\leq 40 \mu\text{m}$) α -quartz ("Q") grains in a matrix containing irregular ($\leq 10 \mu\text{m}$) feldspar ("F") and fine clay relict (<1 μm) particles and powder agglomerates. Feldspar crystals could be distinguished from clay relict particles because the aluminum peaks were higher and the potassium peaks lower in the EDS spectra from clay relict particles, compared with those from feldspar.

As shown in Fig. 3, two types of clay relict agglomerates were observed in P1000. EDS detected more potassium, along with aluminum and silicon, in the agglomerates with lighter contrast (in SEI), suggesting that those agglomerates were feldspar-penetrated clay relicts (labeled "C+F" in Fig. 3(a)). On the other hand, the darker agglomerates (labeled "C") contained few or no potassium peaks, suggesting that they were pure clay relicts. At temperatures $\geq 1000^\circ\text{C}$, some regions ("L") appearing dark in BSI showed a morphology suggesting the formation of a liquid in the matrix (Fig. 3(b)). Under this condition, the angular feldspar crystals seemed to disappear and the liquid content to increase with temperature, probably because of gradual melting of feldspar. Pure clay ("C") relict agglomerates could be clearly distinguished from mixed clay-feldspar ("C+F") relicts at $\geq 1100^\circ\text{C}$ (Fig. 4(a)), because of their more contiguous microstructure. Most of the feldspar crystals had dissolved by 1100°C, except a few, large (~1 μm) partially dissolved (indicated by the rounding of their edges) microcline crystals, identified by their SADPs in the TEM (Fig. 4(b)).

In P1000, precipitation of $\gamma\text{-Al}_2\text{O}_3$ and/or primary mullite ($\leq 7 \text{ nm}$) was observed in pure clay relicts, while in feldspar-fluxed regions, mullite crystals were more developed (Fig. 5(a)). Pure clay relicts of P1100 contained small ($\leq 50 \text{ nm}$) mullite crystals (left side of Fig. 5(b)), while clay-feldspar relict regions contained longer ($\leq 0.5 \mu\text{m}$) mullite crystals (right side of Fig. 5(b)). The crystals were identified using SADPs. SEM of P1300 revealed three distinct regions containing different types of mullite: pure clay relicts containing aggregates of primary, scaly type-I mullite ("MI"); feldspar-penetrated clay relicts containing secondary, granular type-II mullite ("MII"); and a matrix of clay, feldspar, and quartz containing longer ($\leq 20 \mu\text{m}$), secondary type-III mullite ("MIII"), as well as type-II mullite (Fig. 6). TEM showed that the contiguous pure clay aggregates contained $\leq 0.1 \mu\text{m}$ cuboidal MI mullite crystals in a glassy matrix (Fig. 7(a)), while the feldspar-penetrated granular microstructure contained a mixture of $\leq 0.1 \mu\text{m}$ cuboidal and longer ($\leq 1 \mu\text{m}$) MII mullite crystals (Fig. 7(b)).

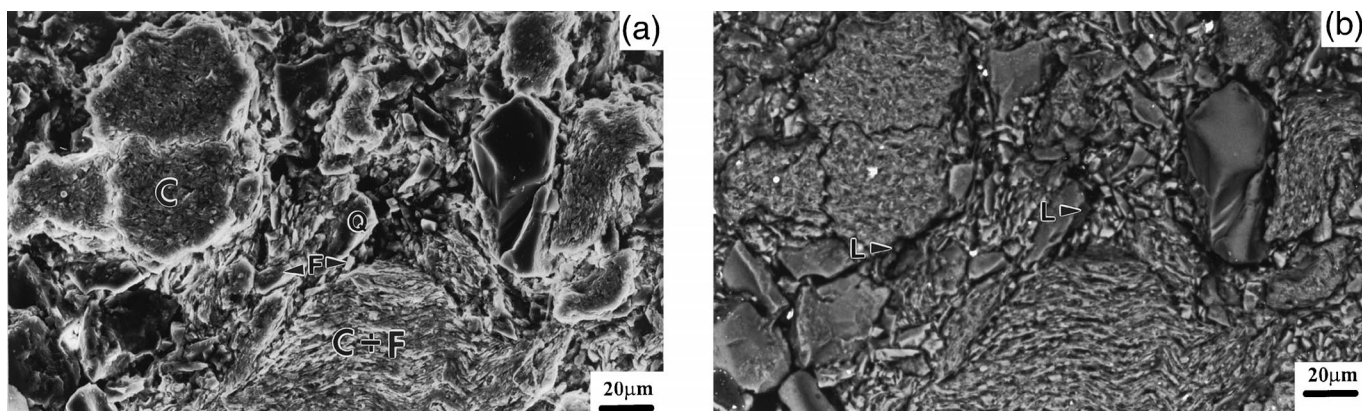


Fig. 3. (a) SEI of etched P1000, showing α -quartz grains (“Q”), clay relict agglomerates (“C”), and feldspar (“F”) in a mixed clay-feldspar relict matrix; note the lighter contrast of clay relict agglomerates (“C+F”) containing feldspar. (b) BSI from the same area in (a), showing dark phase suggesting liquid (“L”) formation in the matrix and also at the boundaries of clay relict agglomerates.

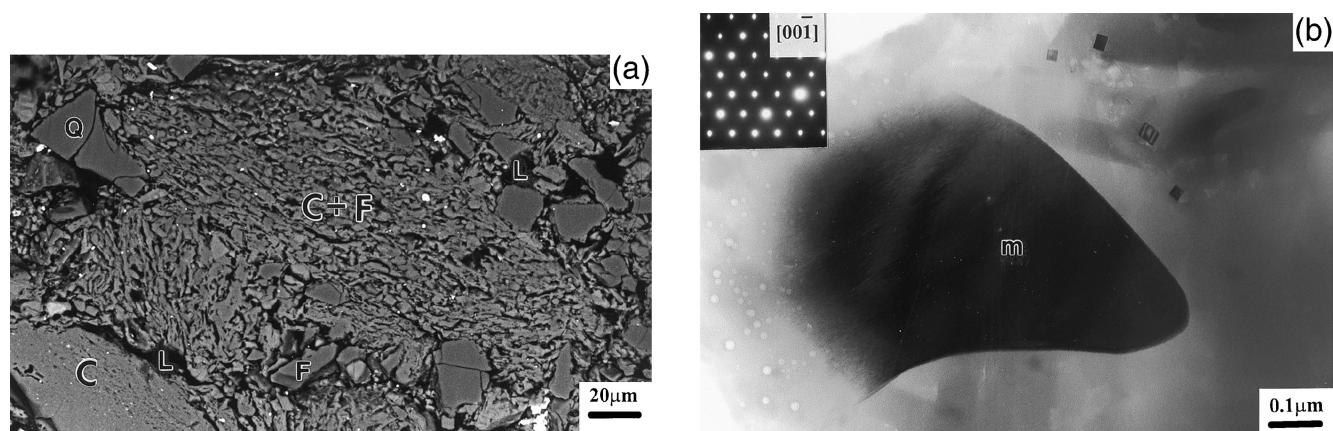


Fig. 4. Microstructures in P1100: (a) BSI showing α -quartz grains (“Q”), pure clay relict agglomerates (“C”), mixed clay-feldspar relict agglomerates (“C+F”), and a partially dissolved feldspar crystal (“F”); note the dark phase suggesting liquid (“L”) formation in the matrix, the boundaries of clay relict agglomerates, and also in the mixed clay-feldspar relicts. (b) BF-TEM image and a corresponding [001] SADP of a partially dissolved microcline crystal (“m”).

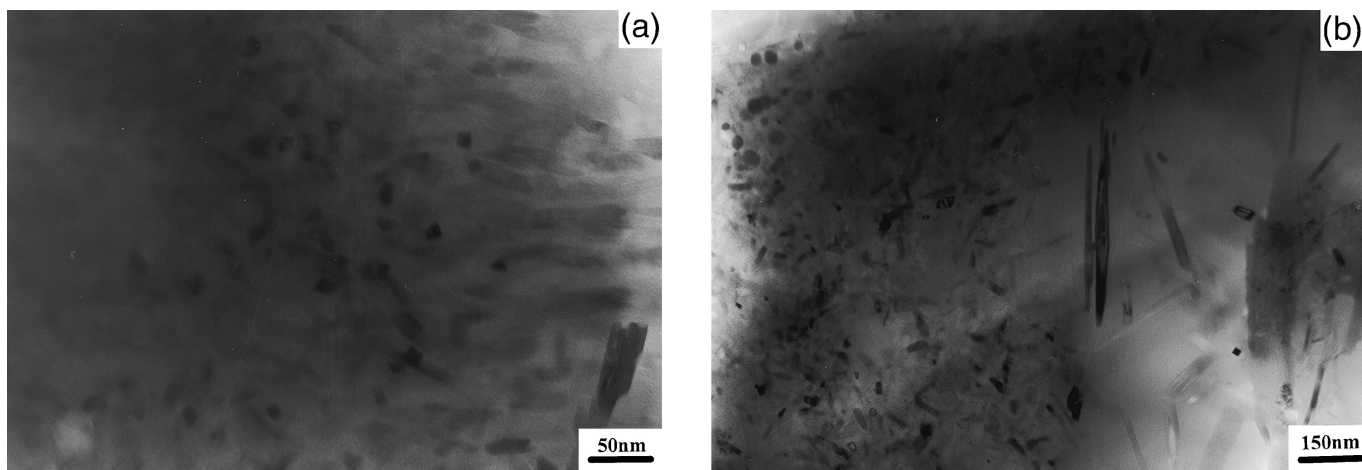


Fig. 5. BF-TEM images of clay relicts (left side of each figure) adjacent to feldspar-penetrated relicts (right side); primary mullite crystals on the left side are smaller than secondary mullite crystals in feldspar-fluxed areas: (a) P1000 and (b) P1100.

Angular α -quartz crystals in P1100 indicated that α -quartz dissolution had not yet begun, although after 1300°C rounding of the edges of the α -quartz crystals indicated their partial dissolution. Above 1300°C, bubbles formed throughout the microstructure, and quartz grains had partially dissolved. Figure 8(a) shows bubbles formed in samples fired at 1400°C. In P1500, EDS of regions close to bubbles revealed the presence of aluminum and

silicon only, suggesting that those regions were clay relicts. The bubble-free matrix contained aluminum, silicon, and potassium, indicating that it was feldspar-derived glass. The microstructure of porcelain fired at 1500°C consisted of long (>10 μm) mullite needles (M) in a potassium silicate glass, and extensive cracking of quartz (labeled “SiO₂”) grains indicated its possible¹⁵ transformation to cristobalite (Fig. 8(b)).

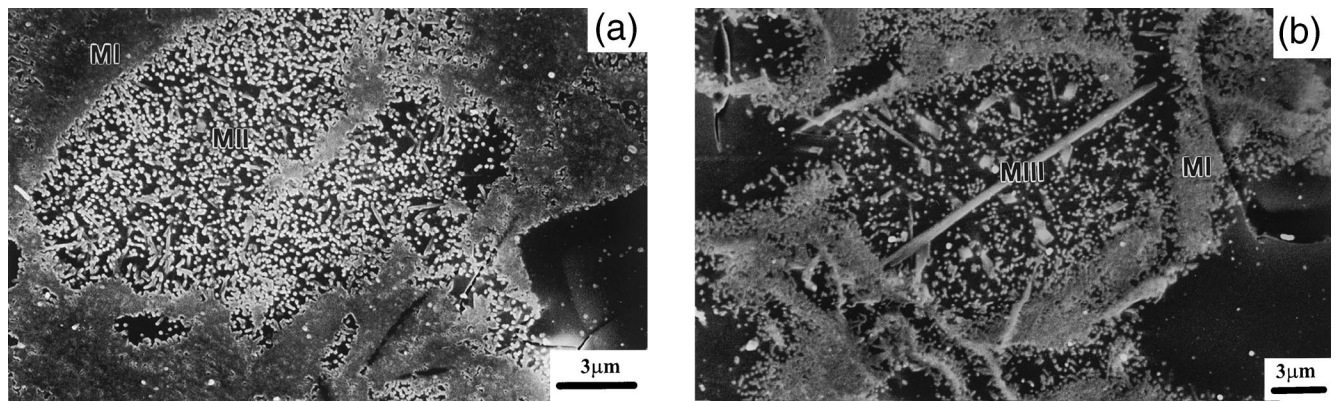


Fig. 6. (a) SEI of etched P1300, showing scaly mullite (“MI”) and granular mullite (“MII”) formed in pure clay relict and feldspar-penetrated clay relict agglomerates, respectively. (b) SEI from the same sample, showing an elongated ($\sim 20 \mu\text{m}$) mullite crystal (“MIII”) formed in the matrix containing mixed clay-feldspar grains.

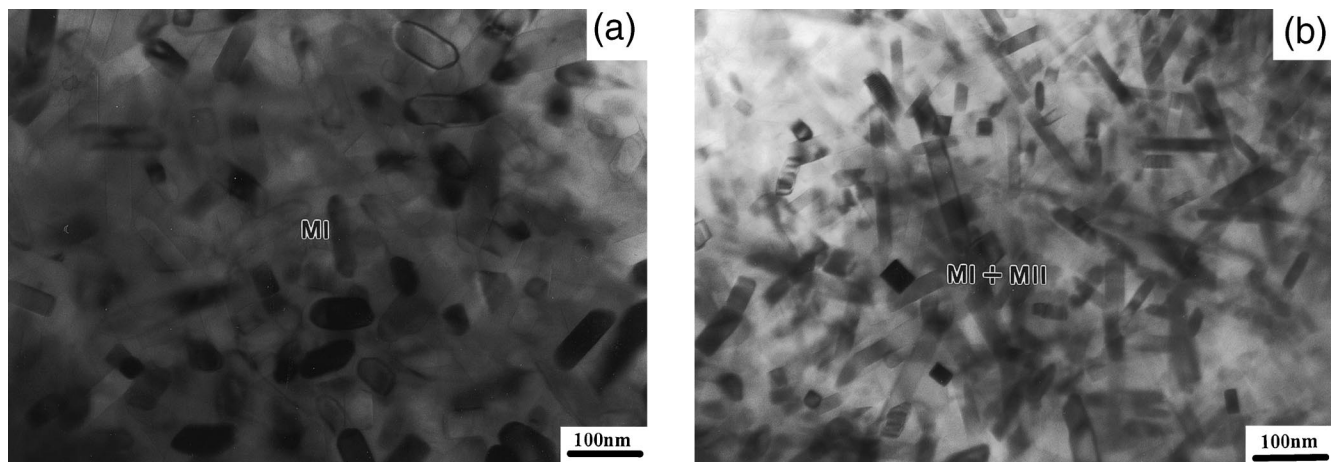


Fig. 7. BF-TEM images of P1300: (a) pure clay relict, showing cuboidal primary mullite crystals and (b) feldspar-penetrated clay relict containing longer, secondary mullite crystals, along with cuboidal, primary mullite crystals.

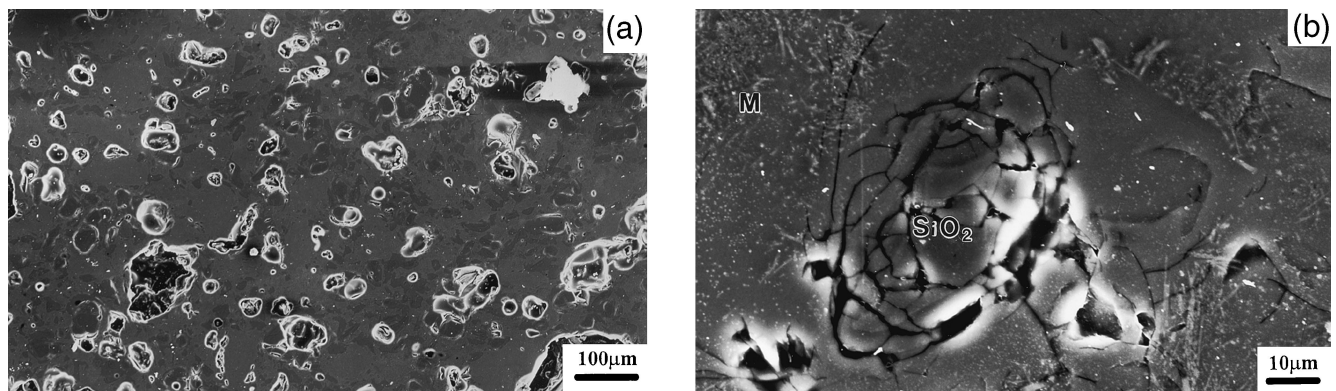


Fig. 8. SEI of (a) etched P1400, showing bubbles formed on overfiring, and (b) etched P1500, showing mullite needles (“M”) in potassium silicate glass. Note the cracked quartz grain (“ SiO_2 ”), indicating the partial transformation of quartz into cristobalite.

Semiquantitative EDS revealed that the $\text{Al}_2\text{O}_3\text{:SiO}_2$ wt% ratio for primary (MI) mullite was 83:17 to 89:11 at $\leq 1300^\circ\text{C}$; for secondary (MII and MIII) mullite, the ratio was 71:29 to 75:25. At 1500°C , most of the mullite crystals contained 87–90 wt% Al_2O_3 and 13–10 wt% SiO_2 , independent of their size and origin. In most cases, the glass close to quartz grains contained SiO_2 only, whereas the glass composition varied in the matrix throughout the microstructure. For example, the K_2O content of glass in clay relicts (which contained primary MI crystals) varied from 0 to 9 wt%, whereas in feldspar relicts (i.e., in the vicinity of secondary MII and MIII crystals), it varied from 0 to 13 wt%. The decreased

intensity of XRD peaks for mullite indicated its partial dissolution at $>1400^\circ\text{C}$.

IV. Discussion

The increased density of pellets fired at $1100^\circ\text{--}1300^\circ\text{C}$ (Fig. 1) is associated with liquid formation at $\sim 985^\circ\text{C}$, via the $9.5\text{K}_2\text{O}\cdot 10.9\text{Al}_2\text{O}_3\cdot 79.8\text{SiO}_2$ (in wt%) eutectic, and feldspar melting at $\geq 1100^\circ\text{C}$, which filled the pores and densified the bodies.¹³ The decreased density at $>1300^\circ\text{C}$ results from gas evolution,

leading to bubbles in the microstructure (Fig. 9(a)). The bubbles form in feldspathic regions of overfired bodies, which contain OH^- groups and nitrogen.¹⁹ Bubbles are observed in clay relicts and not in feldspar-derived glass, which suggests that bubbles may form in less viscous regions (such as feldspar melt) in the early stages of overfiring.²⁰ However, at higher temperatures ($>1400^\circ\text{C}$), the reduced viscosity facilitates release of entrapped gases from these regions, although they remain in more viscous clay relicts.

DTA of as-mixed porcelain powders revealed the reactions of the kaolinite only. The continuous endothermic drift of nepheline syenite at $>500^\circ\text{C}$ is a result of its gradual melting. Consistent with DTA results, XRD of nepheline syenite revealed the presence of >95 vol% glass at 1200°C and a small amount ($<5\%$) of leucite, which dissolved at $<1400^\circ\text{C}$. The dissolution of leucite at a lower temperature than reported for pure potash feldspar (1530°C) may result from the presence of nepheline, affecting its dissolution temperature.¹⁰

McConville *et al.*⁷ studied microstructural evolution in pure kaolinite, using TEM, and reported spinel ($\gamma\text{-Al}_2\text{O}_3$) formation at $>900^\circ\text{C}$ and primary mullite at 1000°C . In the present work, XRD indicated mullite formation at a temperature $<1100^\circ\text{C}$.¹⁵ The lower viscosity of porcelain bodies because of the fluxing action of feldspars facilitates more rapid growth of crystals than in pure clay bodies; therefore, the small (≤ 7 nm) crystalline features observed by TEM in P1000 may be the spinel phase in pure clay relicts, while the larger (≤ 30 nm) crystals observed in some regions are the secondary MII mullite crystals in feldspar-penetrated clay relicts. Lundin¹⁵ demonstrated that mullite crystals grow from the outer surface of the clay relict into the feldspar relict, suggesting that primary (type-MI) mullite may act as a seed for the nucleation of secondary (type-MII) mullite.

In the present study, three types of regions (which may crystallize mullite) were observed: pure clay relict agglomerates containing type-MI mullite, feldspar-penetrated clay agglomerates

additionally containing type-MII mullite, and mixtures of clay and feldspar particles containing type-MII and type-MIII mullite in the matrix (Fig. 6). Type-I mullite regions contained clusters of small (≤ 0.1 μm) crystals and were primary mullite, because they formed first at $<1100^\circ\text{C}$; type-II mullite regions had a granular morphology, and the crystals were shorter than those of type MIII, which were highly elongated and acicular (Fig. 7).

The observed variation in the morphology and size of mullite crystals is explained by the gradient in viscosity of the relevant matrix and subsequent, more-rapid mass transport.⁶ Mullite formation and its distribution in the feldspar and clay relicts is determined by diffusion processes within the reaction layer between the feldspar and the clay relicts. The diffusion process depends on the concentration gradients and the diffusion rates of K_2O and Al_2O_3 . Feldspar melts at a lower temperature than the other constituents in the body, and mixtures of clay and feldspar grains have the lowest viscosity. Similarly, clay relict agglomerates containing feldspar are more fluid than the agglomerates containing no feldspar. Consequently, some type-III mullite crystals may grow longer in the least-viscous clay-feldspar relict mixtures than the type-MII mullite in the more-viscous clay relict agglomerates containing some feldspar. Type-I mullites formed in the pure clay relict agglomerates are the smallest because of the highly viscous matrix. A box diagram of phase evolution in triaxial porcelain, based on the present XRD study, is shown in Fig. 9. Fig. 10 shows the microstructural evolution of triaxial porcelain, based on the present SEM and TEM studies

The dissolution of quartz depends on its grain size and also on the type of feldspar used.^{1,2,15,21} Lundin¹⁵ reported that the transformation of quartz into cristobalite begins at $\sim 1200^\circ\text{C}$, with the formation of an outer zone around the quartz grains; however, in the present study, cristobalite was only observed at $>1400^\circ\text{C}$.

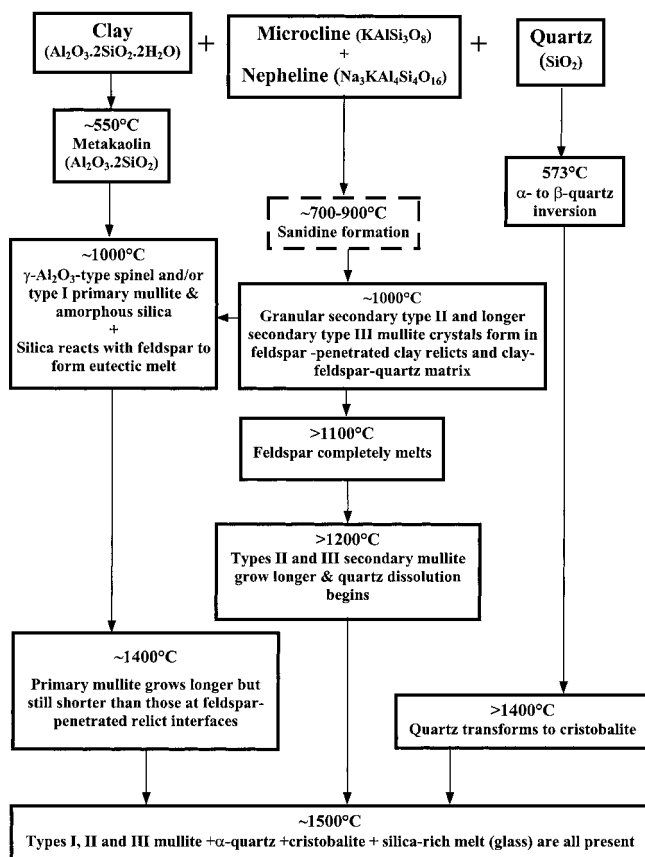


Fig. 9. Box diagram of suggested phase evolution in triaxial porcelain, based on XRD, SEM, and TEM results.

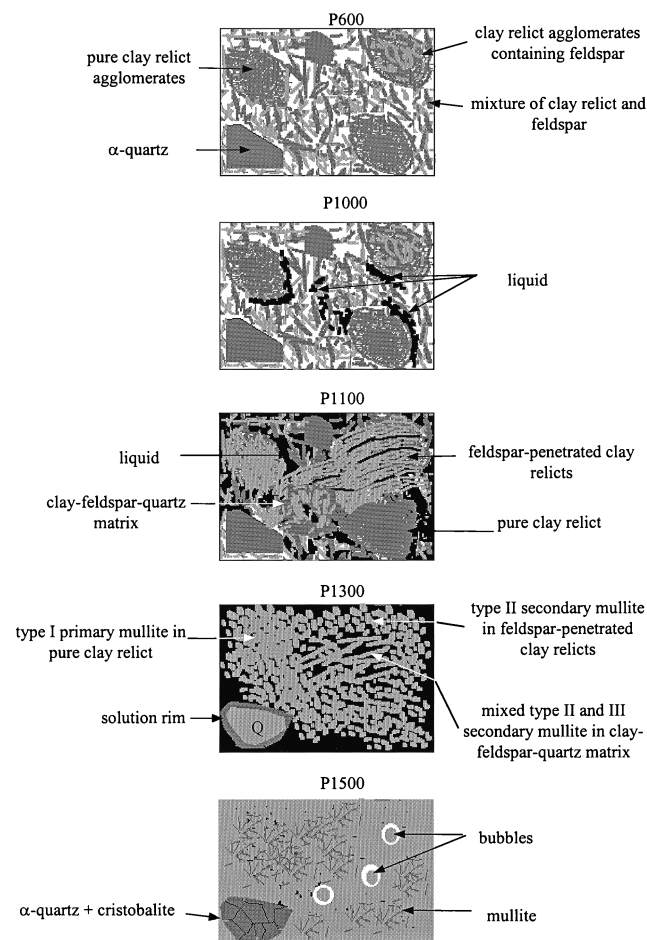


Fig. 10. Schematic illustration of the suggested microstructural evolution in triaxial porcelain.

Hermansson and Carlsson²² found that the composition of glass was consistently the same ($76\text{SiO}_2 \cdot 16\text{Al}_2\text{O}_3 \cdot 7\text{K}_2\text{O} \cdot 1\text{CaO}$ (wt%)), whereas Klykova *et al.*²³ reported the presence of three varieties of glass, different in origin and proportion of aluminum and silicon oxides; however, no quantitative information was given. In commercial porcelains fired at 1200°C , Iqbal and Lee⁶ reported a heterogeneous glass of varying K_2O and Al_2O_3 contents throughout the microstructure. In the present study, at $<1300^\circ\text{C}$, the glass close to α -quartz was pure SiO_2 and, as expected, less K_2O was detected in regions containing primary mullite (i.e., clay relicts) than in the vicinity of secondary mullite crystals (i.e., in feldspar-penetrated clay relicts). The Al_2O_3 content also varied throughout the microstructure. Below 1300°C , the chemical composition of primary mullite crystals was Al_2O_3 -rich, while secondary mullite crystals were relatively poor in Al_2O_3 . The reasons for the observed variation in chemical composition may be the different glassy environments (in clay, feldspar relicts, and their mixtures) in which the crystals are embedded.⁶

V. Conclusions

Based on XRD/SEM/TEM analysis, unfired but shaped porcelain bodies were heterogeneous mixtures of feldspar, and particles and agglomerates of kaolinite, along with α -quartz. Clay dehydroxylated at $\sim 550^\circ\text{C}$. Metastable sanidine formed at $>600^\circ\text{C}$ and dissolved at $>900^\circ\text{C}$. Liquid formed at $\sim 1000^\circ\text{C}$, via the K_2O - Al_2O_3 - SiO_2 eutectic, and increased in amount with temperature, first because of feldspar melting (at $>1000^\circ\text{C}$) and later (at $>1200^\circ\text{C}$) because of quartz dissolution. Primary type-I mullite precipitated from pure clay relicts at $\sim 1000^\circ\text{C}$ and increased in size with temperature. Granular, secondary type-II mullite formed in feldspar-penetrated clay relicts and elongated, secondary type-II, as well as type-III, mullite in a mixed clay-feldspar matrix. Mullite crystal size increased from the pure clay relicts to the mixed clay-feldspar matrix because increasing feldspar content made the liquid more fluid, facilitating mass transport and enhancing crystal growth. The decrease in density at $>1300^\circ\text{C}$ resulted from evolved gas that led to bubble formation. Above 1400°C , α -quartz partially transformed to cristobalite. In general, at $<1300^\circ\text{C}$, the glass close to α -quartz crystals was silica, and in the matrix glass, the K_2O and Al_2O_3 contents varied throughout the microstructure, indicating the local heterogeneity of glass composition in porcelain bodies.

Acknowledgments

We thank the EPSRC, United Kingdom, for funding this research, through Grant No. GR/L 71780, and P. F. Messer and B. Lye for helpful discussions.

References

- ¹A. A. Klein, "Constitution and Microstructure of Porcelain," National Bureau of Standards Tech. Paper No. 3-38, 1916-17.
- ²P. Rado, "The Strange Case of Hard Porcelain," *Trans. J. Br. Ceram. Soc.*, **70**, 131-39 (1971).
- ³S. B. Vazquez, J. C. M. Velazquez, and J. R. Gasga, "Alumina Additions Affect Elastic Properties of Electrical Porcelains," *Bull. Am. Ceram. Soc.*, **77** [4] 81-85 (1998).
- ⁴Y. Kobayashi and E. Kato, "Lightening of Alumina-Strengthened Porcelain by Controlling Porosity," *J. Jpn. Ceram. Soc.*, **106** [9] 938-41 (1998).
- ⁵S. T. Lundin, "Electron Microscopy of Whiteware Bodies"; pp. 383-90 in *Transactions of the IVth International Ceramics Congress* (Florence, Italy, 1954).
- ⁶Y. Iqbal and W. E. Lee, "Fired Porcelain Microstructure Revisited," *J. Am. Ceram. Soc.*, **82** [12] 3584-90 (1999).
- ⁷C. J. McConville, W. E. Lee, and J. H. Sharp, "Microstructural Evolution in Fired Kaolinite," *Br. Ceram. Trans.*, **97** [4] 162-68 (1998).
- ⁸C. L. Norton, "The Influence of Time on Maturing Temperature of Whiteware Bodies: II," *J. Am. Ceram. Soc.*, **14**, 192-206 (1969).
- ⁹K. H. Schuller, "Reactions between Mullite and Glassy Phase in Porcelains," *Trans. Br. Ceram. Soc.*, **63** [2] 103-17 (1964).
- ¹⁰T. N. McVay, "Physical-Chemical Reactions in Firing Whiteware," *J. Am. Ceram. Soc.*, **19**, 195-97 (1936).
- ¹¹A. Dinsdale, *Pottery Science Materials, Process, and Products*. Ellis Horwood Ltd., West Sussex, U. K., 1986.
- ¹²Y. Kobayashi, O. Ohira, Y. Ohashi, and E. Kato, "Vitrification of Whiteware Bodies in Alumina-Feldspar-Kaolin System," *J. Jpn. Ceram. Soc.*, **100** [5] 743-49 (1992).
- ¹³E. M. M. Salam, P. F. Messer, and W. F. Ford, "Equilibrium Constitution as an Index of the Vitrification of Triaxial Whitewares," *Trans. J. Br. Ceram. Soc.*, **75**, 120-23 (1976).
- ¹⁴W. S. Mackenzie and J. V. Smith, "The Alkali Feldspar: III. An Optical and X-ray Study of High Temperature Feldspar," *Am. Mineral.*, **41** [5-6] 405-27 (1956).
- ¹⁵S. T. Lundin, "Microstructure of Porcelain"; pp. 93-106 in *Microstructure of Ceramic Materials*, Proceedings of the American Ceramic Society Symposium, National Bureau of Standards Miscellaneous Publications No. 257. National Bureau of Standards, Gaithersburg, MD, 1964.
- ¹⁶R. B. Sosman, *The Phases of Silica*. Rutgers University Press, New Brunswick, NJ, 1965.
- ¹⁷L. Mattyasovszky-Zsolnay, "Mechanical Strength of Porcelain," *J. Am. Ceram. Soc.*, **40** [9] 299-306 (1957).
- ¹⁸Y. Ohya, Y. Takahashi, M. Murata, Z. Nakagawa, and K. Hamano, "Acoustic Emission from a Porcelain Body during Cooling," *J. Am. Ceram. Soc.*, **82** [2] 445-48 (1999).
- ¹⁹G. P. K. Chu, "Microstructure of Complex Ceramics"; Ch. 38, pp. 843-44 in *Ceramic Microstructures, Their Analysis, Significance, and Production*. Edited by R. M. Fulrath and J. A. Pask. Wiley, New York, 1968.
- ²⁰A. W. Norris, D. Taylor, and I. Thorpe, "Range Curves: An Experimental Method for the Study of Vitreous Pottery Bodies," *Trans. J. Br. Ceram. Soc.*, **78**, 102-108 (1979).
- ²¹C. W. Parmelee and C. R. Amberg, "Solubility of Quartz and Clay in Feldspar," *J. Am. Ceram. Soc.*, **12** [11] 699-710 (1929).
- ²²L. Hermansson and R. Carlsson, "On the Crystallisation of the Glassy Phase in Whitewares," *Trans. J. Br. Ceram. Soc.*, **77**, 32-39 (1978).
- ²³Y. Klykova, A. Mazurkevich, and V. Panteleyev, "Image Analysis and SEM Studies of Ancient Ceramics and Feldspar Porcelain Structure," *Microsc. Anal.*, **9**, 31-34 (1998). □